IEEE Access
Multidisciplinary | Rapid Review | Open Access Journal

Received August 16, 2020, accepted September 2, 2020, date of publication September 8, 2020, date of current version January 27, 2021.

Digital Object Identifier 10.1109/ACCESS.2020.3022626

Deposit Location Identification Based on Feature Decomposition of High-Resolution Remote Sensing Images

SHULAN TANG[1,2] AND JIANNONG CAO[1]

[1]School of Earth Science and Resources, Chang'an University, Xi'an 710054, China
[2]School of Management, Xi'an University of Finance and Economics, Xi'an 710010, China

Corresponding author: Jiannong Cao (xacjnchan@126.com)

This work was supported in part by the National Natural Science Foundation of China (NSFC): Research on Feature Structured Multi-Scale Analysis Method for Information Extraction of High Resolution Remote Sensing Image under Grant 41571346, and in part by the Project of Shaanxi Provincial Department of Education under Grant 18JK0317.

ABSTRACT In modern mineral exploration applications, remote sensing technologies have been widely used and affirmed by engineering and mineral industries due to their unique technical advantages. With the advancement of remote sensing technologies, multiple geological remote sensing-derived prospecting methods have been developed. With the development of more accurate sensors, the detection band has not been segmented, and the spectral resolution of such sensors is constantly being improved. Thus, the accuracy of remote sensing geological prospecting methods has improved, and geological prospecting results have shifted from being qualitative to quantitative in nature. In this article, high-resolution remote sensing images are used to extract the ore controlling factors of deposits. The color, shape, texture and other image shapes produced by high-resolution remote sensing images are fully exploited to comprehensively mine the available data utilizing mathematics, image processing methods and other technologies to systematically identify prospective target areas. Based on an analysis of the metalloorganic geological characteristics detected in the study area, combined with multisource data such as geophysical and geochemical exploration-derived observations, the proposed remote sensing model describing the deposits in the study area is summarized. The research results show that deposit location identification technologies based on high-resolution remote sensing image feature decomposition have the potential to provide a reliable basis for peripheral exploration and deposit positioning in geological and mineral exploration studies.

INDEX TERMS High-resolution remote sensing image, feature extraction, mineral location, target detection.

I. INTRODUCTION

Remote sensing technology is a necessary means of geological exploration. Traditional remote sensing prospecting methods are generally based on low to medium spatial resolution, multispectral or hyperspectral image data. There are four commonly applied research methods [1]. One is to determine the target area based on experience and visual interpretation. This method is usually applied by remote sensing experts who have many years of experience. The second is to extract geological structures and alteration details from multispectral remote sensing images to comprehensively analyze the regional metalloorganic geological conditions and determine the prospecting target area [2]. This method is usually suitable for researchers who are familiar with the theory and mechanisms behind geologic phenomena and mineralization. Third, computer image processing is used to extract geological information [3]. This method is usually used by researchers who have not specialized in geology-related fields to distinguish metalloorganic characteristics according to computationally interpreted information, and its results are generally not accepted or adopted for geological applications. Fourth, comprehensive analysis of various remote sensing and geological data using mathematical statistical methods is used to conduct comprehensive evaluations [4]. This technique has a strong applicability and a high comprehensiveness. It is a widely used method in remote sensing prospecting. Information extraction is a key step in high-resolution remote sensing image interpretation and recognition. Linear texture information extraction is an important part of

The associate editor coordinating the review of this manuscript and approving it for publication was Zhihan Lv.

information extraction. However, when comparing low- and medium-resolution remote sensing images, the spectral characteristics of ground objects in high-resolution remote sensing images are more obvious. Additionally, spatial structure information, such as the geometric structure and texture of ground objects, is very prominent in geologic applications and makes it possible to achieve more accurate ground target extraction results by only utilizing image information [5]. Pixel-based remote sensing image analysis methods cannot meet the requirements of high-resolution remote sensing image information extraction and have become the bottleneck of large-scale remote sensing applications [6]. The type of target recognition and information extraction urgently needs to shift from being pixel-based to feature-based to make full use of the valuable feature information provided by ground objects in high-resolution remote sensing images.

Although the acquisition technology of high-resolution remote sensing imagery has made remarkable progress, the development of information processing technology for high-resolution remote sensing images is lagging. Compared with low- and medium-resolution remote sensing images, the objects in high-resolution remote sensing images are not only clear and discernible but can also provide an abundance of details [7]. The boundary between adjacent objects is clearer; therefore, images pixels no longer contain several types of ground feature data, such as that of low- and medium-resolution remote sensing images, but rather only reflects the localized properties of ground objects. Although the visual interpretation method can still be used to classify and identify objects in high-resolution remote sensing images, for many images, this undoubtedly requires a large amount of work and takes more time to obtain ground feature data provided by such images [8]. However, if high-resolution remote sensing images are classified by pixel-based methods using computational technologies, the results will often have too much salt and pepper interference, which is not conducive to further remote sensing applications. The original methods used to interpret low- and medium-resolution remote sensing images can no longer adapt to the new characteristics of high-resolution remote sensing images, such as its greater amount of details, resulting in a large number of such images that cannot be effectively and timely processed nor fully fulfil its role, thus further limiting the wide application of high-resolution remote sensing images in various fields. Many scholars have performed numerous studies in this field [9], [10]. Manjunath *et al.* proposed an aerial image query system based on multiscale Gabor features and a texture dictionary; Zhlub extracted the textural features of images using a self-organizing neural network and proposed a remote sensing image retrieval prototype system for atmospheric properties; Agoras established an intelligent high-precision satellite image and aerial image prototype system based on object shapes; and Zhou Yan *et al.* established a shape-based remote sensing image retrieval system [11]. This system adopts a two-step retrieval strategy based on global features and local shape features. It uses simple global features to filter out most of the irrelevant shapes, and a vector approximation method is used to locate the various categories [12]. Although some progress has been made, there are still some shortcomings in the application of content-based remote sensing image retrieval methods, such as single retrieval features and low accuracy and efficiency processing [13].

Existing remote sensing prospecting technologies mainly use multispectral remote sensors with a spatial resolution of one meter to interpret geological information. The computational interpretation method is also relatively mature, and main filtering technologies can extract structural information. The ratio method and principal component analysis method can extract alteration data. The common prospecting model consists of line ring group block comprehensive information. Personnel who are familiar with remote sensing technologies mainly use computationally-derived information to automatically extract one-sided delineation of prospect target areas, while those who are familiar with geology are forced to simply overlay the geological information onto the image. These two methods cannot make remote sensing technology truly serve for prospecting and exploration purposes. Remote sensing applications to geology combine computational technologies, mathematics, and geological theories. How to make better use of available remote sensing technologies for prospecting and exploration is a problem that geologists practicing remote sensing should consider. We cannot simply rely on expert experience nor automated information extraction. We must perform comprehensive analyses and evaluations of remotely sensed data, combined with image characteristics, to fully realize the advantages of mathematics and statistics to extract information from such images. In this article, a high-resolution remote sensing image prospecting method based on image feature decomposition is proposed, which includes extracting the color and texture features of images and calculating the second derivative of image spectrums. The logical superposition analysis method is used to comprehensively analyze the extracted color and texture features and other elements. Through use of fuzzy mathematics theories, element intersections are obtained by the multiplication algorithm. Intersection positions are then considered prospective remote sensing target areas. These results are this study are as follows: make full use of the color, shape, texture and other image shapes provided by high-resolution remote sensing data; fully mine the available data using mathematics, image processing, and other technologies; comprehensively identify prospecting target areas; and provide a reliable basis for the peripheral exploration and deposit positioning of mining areas.

II. REMOTE SENSING TECHNOLOGY AND ITS APPLICATION

A. CONCEPT AND CHARACTERISTICS OF REMOTE SENSING TECHNOLOGY

Remote sensing refers to the use of modern technology and advanced tools to directly receive electromagnetic spectrum

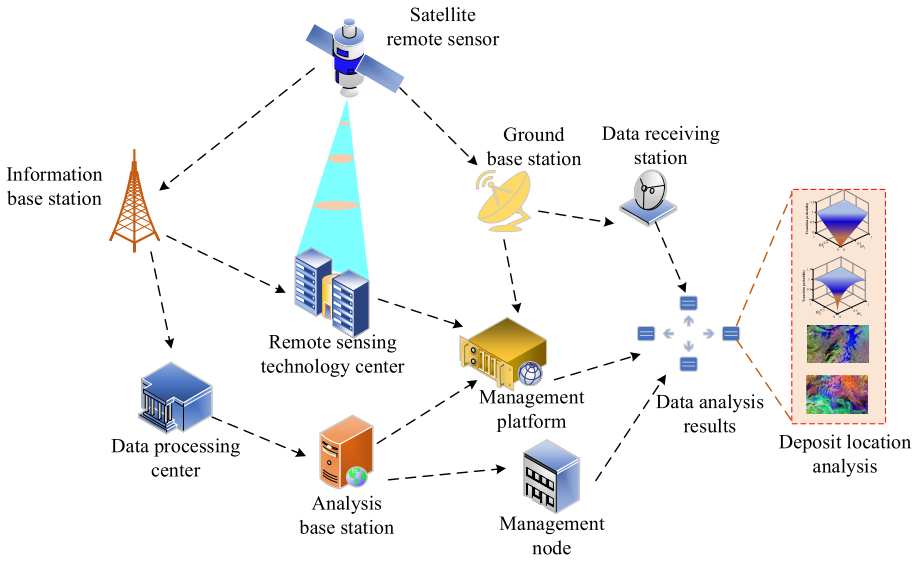

FIGURE 1. The link of remote sensing technologies.

data from targeted objects from a long distance without initiating contact with the target and analyze and interpret the information through transmission, storage and processing; it is considered an emerging comprehensive science. It is a fast and effective method used to acquire large-scale information [14]. Remote sensing technologies are mainly divided into two categories: aerospace remote sensing technology, which mainly refers to the use of satellites to collect data by technicians, and aviation remote sensing technology, which mainly refers to the use of aircrafts and other platforms to measure topography and collect the required data [15]. This technology has been widely used in surveying and mapping. The application principle of remote sensing is as follows; the color objects in the same spectrum differs, and the same object receives different light angles from various positions and at a ranges of times. Under these varied light conditions, the heat absorbed by the object differs. This difference can be magnified in the spectrum, and the position, shape, and nature of the object can be judged by differences in the reflected color [16]. This technology is often used in mineral resource exploration, and the main application method is to combine remote sensing technology with digital virtual technology. This method is mainly used to detect deep underground mineral resources.

The energy measured by optical remote sensing methods comes from solar radiation. Solar radiation passes through the atmosphere to reach the Earth's surface and is reflected back into the sky after interacting with the surface target. After reentering the atmosphere, it is collected by the optical system of a remote sensing imaging sensor and then transmitted to the array of the imaging sensor to convert the light signal into an electrical signal [17]. A series of electronic processes forms a digital image, and the satellite's downlink data channel transmits the image to the ground application system. After receiving the downlink data, the terrestrial application system obtains usable digital images through processing, such as decoding and rearranging. The electromagnetic waves reflected by the surface target already carry the target's spectral information, which is the fundamental basis for remote sensing image interpretation. Figure 1 describes the link of remote sensing technologies.

B. APPLICATION OF REMOTE SENSING TECHNOLOGY FOR IDENTIFYING MINERAL DEPOSITS

There multiple types of geologic structures and rock strata. This not only provides resources but also introduces great difficulties to the development of mineral resources. Because of the complexity of geological strata, traditional mineral resource exploration work cannot meet a variety of exploration tasks, and the distribution of mineral resources is relatively scattered [18]. Exploration studies often require more manpower and funds and cannot guarantee the scientific quality of the results. After the introduction of remote sensing technologies, this problem has been effectively solved. Through remote sensing methods, spectrum analysis of different strata across various mining areas can be performed, and the results are depicted via icons [19]. Through icons, the distribution of various mineral resources can be effectively viewed.

The linear structure of remote sensing imagery can be used to effectively and intuitively display the geological distribution of minerals. Through the analysis of structures, the distribution patterns of geological and mineral resources at the location can be obtained, and the specific distribution location of mineable minerals can identified. Substantial changes in geology and geomorphology can affect the distribution of mineral resources and the probability of mineralization. In areas with large changes in geology and geomorphology, it is often easy to find mineral resources with mining value [20]. However, there is nothing absolute, and

some mineral resources with a high mining value are also widely distributed across secondary faults and joint zones that are oblique or parallel to main faults. The spectrogram displayed by remote sensing technology can effectively show the distribution of mineral resources, and analysis of remote sensing spectrograms can be used effectively understand the structural characteristics and distribution of mineral resources within an area [21]. However, this knowledge alone cannot be used to determine the availability of mineral resources. In determining mining value, more information from spectrograms needs to be digitalized and technically processed, and the resulting spectroscopic analysis diagrams are three-dimensional. After analyzing this diagram, the distribution location of mineral resources can be roughly identified. Such mineral resources prospecting methods greatly reduce the time and manpower required for exploration and improves the efficiency and quality of the efforts.

The color difference displayed along the remotely sensed spectrum represents changes in the physical and chemical properties of mineral beds after alteration or mineralization. The display of this type of variation on the remote sensing spectrum is represented by differences in the color tone, which is altered to fit various scales on the spectrum. Through analysis of these effects, the locations of mineralization and alteration deposits can be accurately identified. Multiband remote sensing imagery, such as infrared aerial remote sensing images, are used to interpret geological bodies related to mineralization, such as rocks, strata, structures and wall rock alteration zones, and mineral information can be extracted using visual interpretation and remote sensing processing technology. At the same time, machine translation can be used to comprehensively process the results of mineral pattern interpretations and geophysical and geochemical exploration data, delineate mineralization prospects, and propose future exploration areas and targets.

III. FEATURE EXTRACTION BASED ON HIGH-RESOLUTION REMOTE SENSING IMAGES

A. PRINCIPLE OF REMOTE SENSING IMAGE FEATURE EXTRACTION

Dimensional change is a calculation that is often used in the postprocessing of captured remotely sensed images. Because traditional remote sensing feature extraction has the characteristics of multidimensional spatial analysis and the ability to extract pixel features in terms of time and frequency, this method can be used to analyze and extract the local features of remotely sensed images in time and process frequency changes, and it has been increasingly widely used in the postprocessing of remote sensing image capture [22]. Traditional image capture postprocessing uses frequency pixel restoration analysis in processing two-dimensional frequency changes to one-dimensional space and extracts important features of the original image's multipixel main features image.

For $R_0(\Delta t, t \geq 0)$ in the postprocessing of the captured image pixels, perform image pixel restoration $f \rightarrow (r_0 f, \Delta_1 f, \Delta_2 f, \ldots)$ for the pixel range of different subbands. The subband $\Delta_t f$ in multidimensional space contains a pixel space of 2^{-2t} as its main feature.

In the process of restoring remote sensing image pixels, the set of $\beta_G(\varphi_1, \varphi_2)$ is set in a two-dimensional space with a pixel space of 2^{-2t}, and the parameter of the restored image pixel corresponding to function β_G is calculated to obtain a similar set.

$$G = \left[\tau_1/2^t, (\tau_1+1)/2^t\right] \times \left[\tau_2/2^t, (\tau_2+1)/2^t\right] \quad (1)$$

This type of calculation is applied for image pixel restoration G of a specific algorithm. Following the change in the t similarity segmentation parameters τ_1 and τ_2, smooth segmentation from the parameter to the cube level can be realized, and the feature extraction of image pixel restoration can be further analyzed.

$$\Delta_t f \rightarrow (\beta_G \Delta_t f)_{G \in G_2} \quad (2)$$

Let $T_G f(\varphi_1, \varphi_2) = 2^t f(2^t \varphi_1 - \tau_1, 2^t \varphi_2 - \tau_2)$ normalize the pixel value f; the G parameter function calculated from (2) will be $[0, 1]^2$. In the calculation process at this stage, each result of the calculation is normalized to the same unit pixel feature.

$$g_G = (T_G)^{-1}(\omega_G \Delta_t f), \quad G \in G_t \quad (3)$$

The normalization operation of pixels can gather the pixels of postprocessing, which lays the foundation for image fusion extraction, and any calculation result is analyzed in the pixel set. Under the condition of normalized pixels, a set of basic pixel units ζ_ε forms the orthogonal basis on $L^2(R^2)$. A set of pixels are selected for the postprocessing of capturing remote sensing images. After time-frequency filtering, any one of the generated high-feature pixel parameters f contains the determined boundary function points of image restoration, and the unique point position is determined according to the time and frequency identified in pixel processing. The width of the border zone can be set to 2^{-2t}, and the analysis of the ridge extracted from the remote sensing image fusion shows that the time and frequency bandwidth is similar to the shape of the ridge. When the time and frequency bands of one of the pixels are divided and overlapped with each other, a new empty set is generated. In addition, with the improvement of calculation accuracy, the boundaries of the segmentation zone become increasingly parallel, and the equal boundary segmentation segment is the value that needs to be input [23]. The features of images are extracted after analyzing ridges extracted from remote sensing image fusion. Any calculation parameter can be obtained from the set of orthogonal image pixels.

$$g_G = \sum_{\varepsilon} \alpha(\zeta, G)\zeta_\varepsilon \quad (4)$$

The calculation in formula (4) can be used to normalize any pixel to its spatial position.

$$h_G = (T_G) g_G, G \in G_t \quad (5)$$

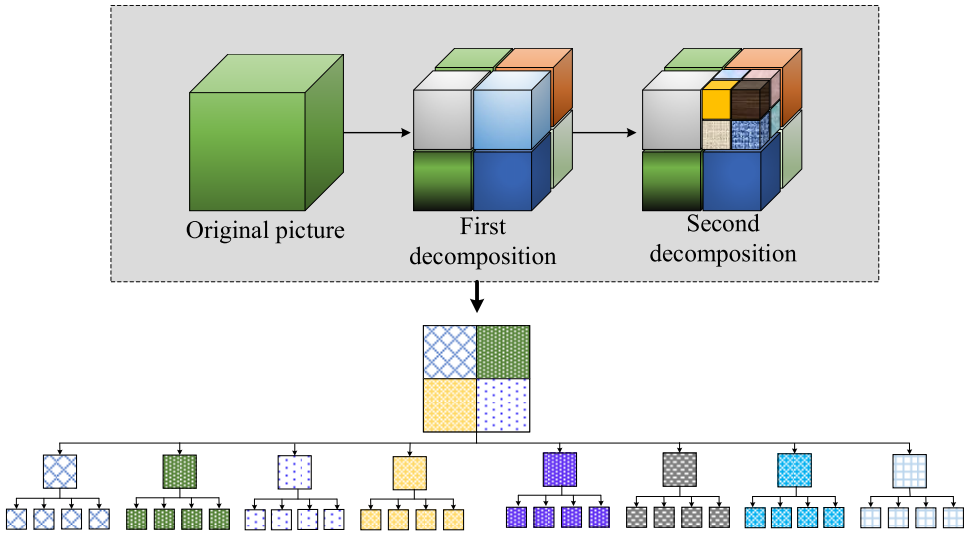

FIGURE 2. Schematic diagram of cross tree decomposition.

Using formula (5), the calculated result can be used as the inverse operation of the image feature fusion boundary.

$$\Delta_t f = \sum_{G \in G_t} \omega_G - h_G \tag{6}$$

We incorporate formula (6) and use the image pixel reconstruction formula to reconstruct the time and frequency.

$$f = r_0(r_0 f) + \sum_{t>0} \Delta_t(\Delta_t f) \tag{7}$$

B. BASIC FEATURE EXTRACTION OF REMOTE SENSING IMAGES

Because remote sensing images are generally stored in large-formats as multitarget complex images, retrieval performed by a similarity match between the query image and the local area of the target image, which determines that most remote sensing image retrieval tasks are subimage-oriented retrievals. To this end, remote sensing images must be divided into blocks, which also differs from remote sensing image retrieval and multimedia and medical image retrieval. To ensure retrieval accuracy, it is necessary to ensure a certain block overlap rate [24]. The overlap ratio refers to the maximum ratio of the area of all subblocks that is arbitrarily extracted from the image with the same size as the subblock after the image passes through a certain block level. Since remote sensing image retrieval is oriented towards subimages, theoretically, the higher the overlap rate is, the more accurate the retrieval will be. First, a total of 12 filters across 3 frequencies and 4 directions are convolved with the image to obtain 12-dimensional texture features. Then, the average (ϑ) and variance (χ) of each 12-dimensional texture feature are calculated as the image texture characteristics, denoted as:

$$F_{texture} = \{(\vartheta_1, \chi_1), (\vartheta_2, \chi_2) \ldots (\vartheta_{11}, \chi_{11}), (\vartheta_{12}, \chi_{12})\} \tag{8}$$

where ϑ is calculated as follows:

$$\vartheta = \frac{\sum_{\alpha=1}^{i} \sum_{\beta=1}^{i} H(\alpha, \beta)}{i \times i} \tag{9}$$

$$\chi = \sqrt{\frac{\sum_{\alpha=1}^{i} \sum_{\beta=1}^{i} (H(\alpha, \beta) - \vartheta)^2}{i \times i}} \tag{10}$$

For the same feature, even if it is depicted in the same type of image, if it is acquired at different time phases, its spectral information may also be quite different. Therefore, this article does not use the average value of each subimage as the image tone but rather uses the variance and third-order moments of each subimage. A schematic diagram of the cross tree decomposition process is shown in Figure 2.

C. DEPTH FEATURE EXTRACTION OF REMOTE SENSING IMAGE

Because depth features can describe higher-level semantic information and the extraction speed is very fast after the network model has been trained, depth features are very suitable for addressing remote sensing image retrieval problems. The general extraction method of deep features uses the labeled data to train a network to obtain a trained network model, removes the last layer used for classification, and inputs the image of the feature to be extracted into the network [25]. Each layer in the network can be regarded as the feature description of the original image being the image feature. Because the receptive field sizes of the convolutional layers of different depths of the network are different and the local area sizes of the corresponding original images vary, the abstraction of images for different convolutional layers differs. The output of the convolutional layer is then a feature map of the local description of the impression [26]. Therefore, it is usually necessary to combine the encoding method to perform

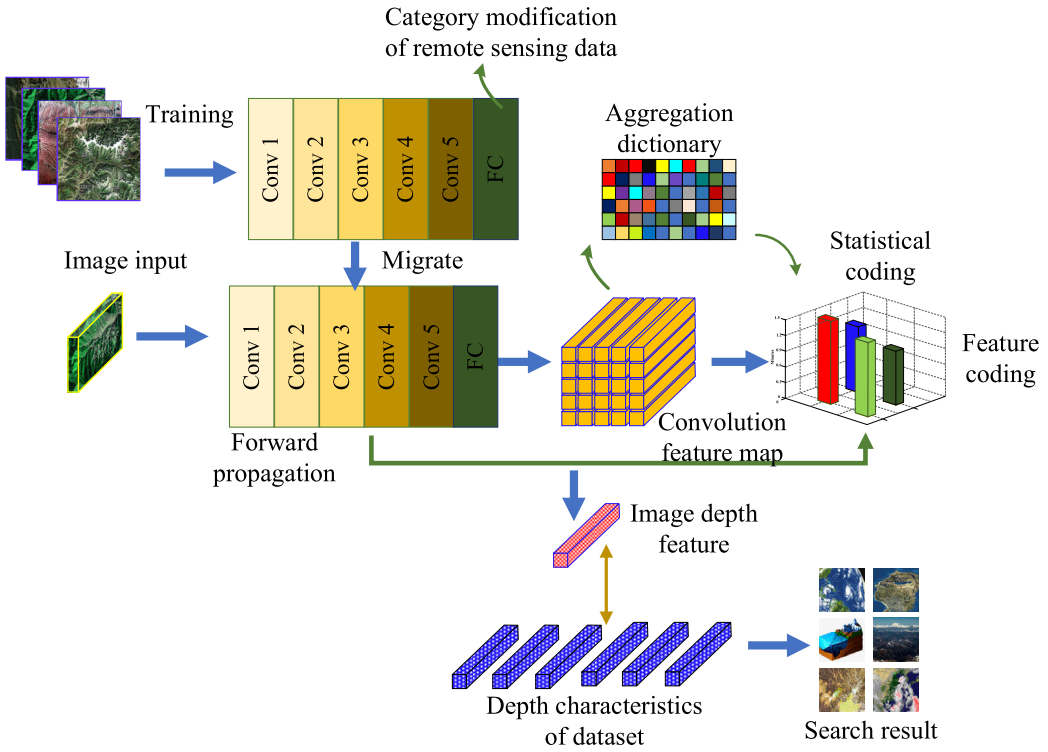

FIGURE 3. Schematic diagram of the whole process of the depth feature extraction.

dimensionality reductions to obtain the feature vector; the encoding method will also have an impact. The feature of the fully connected layer is a global description, which is usually more abstract than the feature of the convolutional layer. The output is a feature vector, which can be directly used as a global feature of the image. These two depth feature methods are used in the overall process of remotely sensed imagery content retrieval. A schematic diagram of the whole process of depth feature extraction is shown in Figure 3.

As shown in Figure 3, the features of the convolutional layer are extracted through the network, and then feature encoding is performed to obtain the depth features. The retrieval results are obtained by sorting or directly extract the fully connected layer as the depth feature. Then, the similarity is measured to obtain the retrieval results, excluding that of the difference layer characteristics. Different network structures, due to their varied structural characteristics, will have different depth characteristics. Since the existing network structure is obtained from natural image training, and because the remote sensing images have various visual characteristics different from natural images, such as perspective, illumination, and rotation, it is necessary to allow the network model to extract features that are more suitable for describing remote sensing images [27]. Remote sensing images are retrained and fine-tuned to achieve the desired results. Next, the depth feature extraction method in remote sensing images is introduced by the feature description methods and characteristics of different layers, which are then retrained and fine-tuned. At the same time, a multispace-scale depth feature is proposed [28]. The influence of various network structures on the depth characteristics of remote sensing images will be analyzed in detail in subsequent experiments.

Figure 4 shows a schematic diagram of the pooling calculation. The value of each pixel in the output feature map is obtained by the convolution operation of the local area of the input layer, so each pixel value is a description of the local area of the previous layer, and it can correspond to the receptive field of the original image layer by layer, as shown in Figure 4 (a). The size of each feature map is determined by the input image and filter sizes, and the number of output feature map channels is determined by the number of convolution kernels determined during network structure design. The deeper the convolutional layer is, the larger its receptive field corresponds to the original image area. Therefore, the deeper the number of layers, the stronger the abstraction of the convolutional layer's features will be, and the characteristics of the description are transformed from detailed information, such as structure, to higher-level semantic information.

Convolution and pooling calculation area mapping; (b) Schematic diagram of maximum pooling and average pooling calculation.

Since the fully connected layer is a vector and matrix multiplication operation, after the network structure is fixed, the size of the input image must be fixed, but this requirement ignores the size of the input target. Therefore, pooling is carried out with reference to the idea of spatial

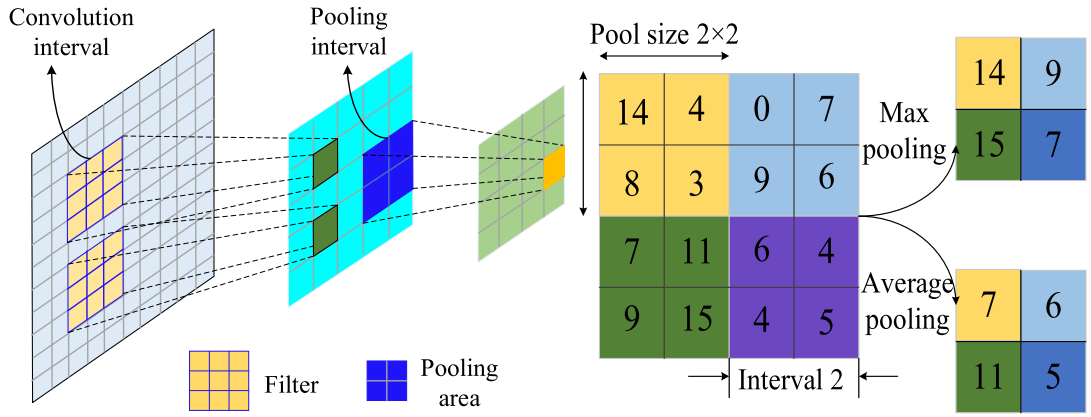

(a) Convolution and pooling calculation area mapping; (b) Schematic diagram of maximum pooling and average pooling calculation.

FIGURE 4. Schematic diagram of the pooling calculation.

pyramid matching. As shown in Figure 4(b), the spatial pyramid method is used to perform pooling operations with different window sizes. The SPP layer dynamically adjusts the size and step length of the pooling window according to the size of the input feature map so that the size of the original input image is not restricted by the network structure, and at the same time, it can obtain convolution features with more spatial information.

The fine-tuned network can be used to extract deep features that can describe the high-level semantic information provided by remote sensing images. Subsequent experiments show that using this feature for content-based remote sensing image retrieval can obtain results superior to previous methods. The overall fine-tuning steps and the steps to extract features using the fine-tuned network model and use them for retrieval are shown in Figure 5.

The structure of the multiscale convolutional neural network is shown in Figure 6. These data are input into the corresponding convolutional layer, the multiscale features are extracted, and the feature maps of different scales are reduced through the different steps of the pooling function so that they are consistent in the two dimensions and merged in the depth dimension. The results are then input into the fully connected layer for classification [29], [30]. In the network model training process, the convolutional layers of 3 different scales are trained simultaneously, the probabilities of each category are mapped in the fully connected layer after feature fusion, and finally, the predicted category is obtained. The loss function is calculated with the true value of the target uniformity, and then backpropagation is performed to update the parameters in each model component [31]. The overall network error is determined by the parameters in the 3 scale roll layers, which ensures the effective function of the features at different scales based on the classification results; the overall performance of the entire network is thus improved.

IV. EXPERIMENTAL VERIFICATION

A. OVERVIEW OF THE STUDY AREA

The study area has a tropical rainforest climate with a high temperature, a high humidity, and a large amount of rainfall. The annual temperature is above 30°C, and the absolute and relative humidities are both high, with an average value greater than 70%. The landforms in the area are mostly hilly landforms with steep mountains, developed gullies and streams. It has a thick vegetation cover, and the altitude mostly ranges between 100 and 700 m. The landforms in the area can be roughly divided into hills and alluvial plains, and the relative elevation difference of the mining area is close to 600 m. Most of the area is covered by a dense tropical rainforest with a well-developed water system and abundant water resources. A large area of Mesozoic basic and ultrabasic intrusive rocks are exposed in the study area, and a small number of Mesozoic-Cenozoic continental margin clastic rocks are exposed. The widely distributed basic-ultrabasic rocks laid the material foundation for the formation of laterite weathered crust nickel silicate deposits in the region. The climate in the area is hot, with sufficient rainfall and strong biochemical weathering forces. Various degrees of laterite weathered crusts are developed on top of the ultrabasic rock masses, which create favorable conditions for the formation of nickel deposits in the laterite weathered crust. The sample data used in the experiment are hyperspectral remote sensing imagery collected from a certain area, and it contains 235 bands and five types of image information, namely, grain, depression, mountain, grassland and lake classifications. The training samples and test samples were classified according to a ratio of 5:2. The maximum optimized number of the genetic algorithm is 600, the original category is 30, the intersection probability is 0.6, and the mutation probability is 0.08.

B. ESTABLISHMENT OF REMOTE SENSING PROSPECTING MODEL

Under the background of basic geological mineralization, the contents of remote sensing prospecting model studies have mainly included image processing and thematic information extraction. The process of extracting thematic information is the process of model building. By using human-computer interaction-derived interpretation methods, remote sensing geological rock mass information,

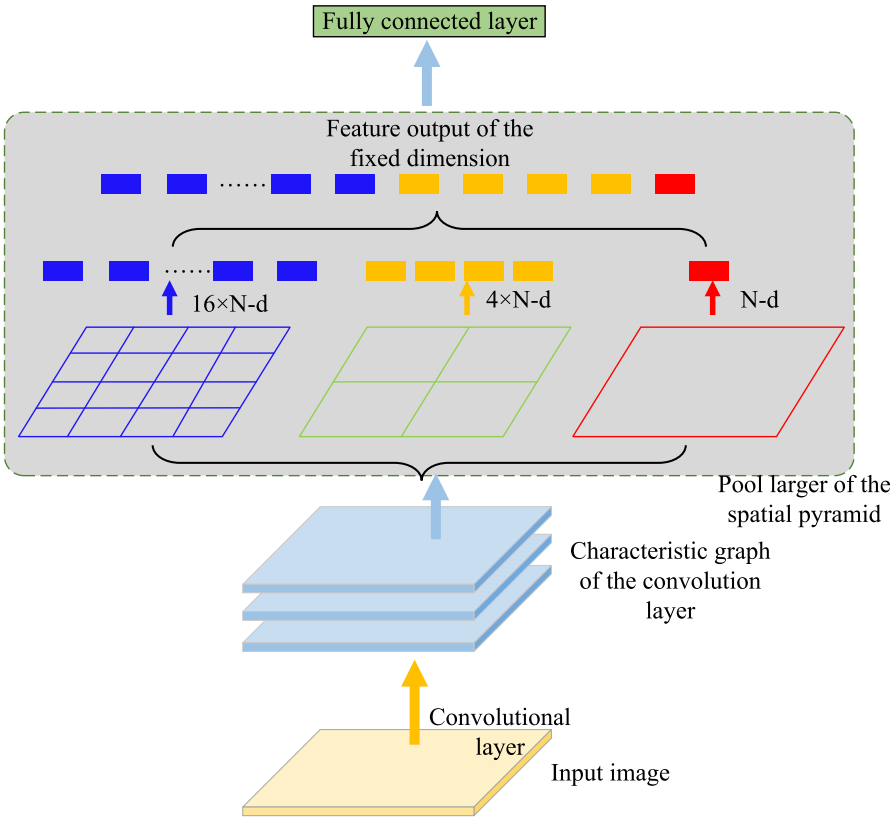

FIGURE 5. Schematic diagram of the spatial pyramid pool structure.

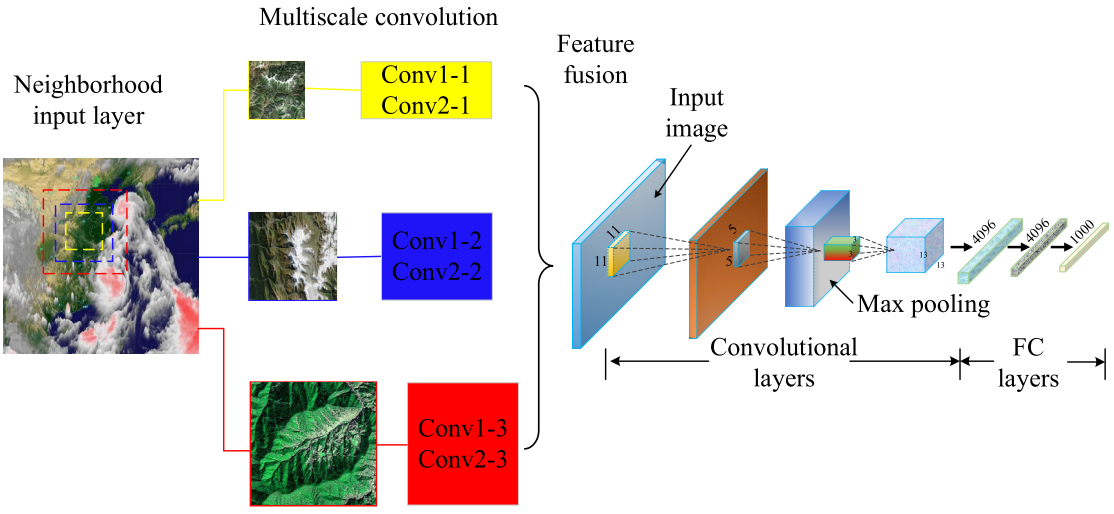

FIGURE 6. Structure of the multiscale convolution neural network.

structural information, mineralization information and other prospecting information are extracted and combined with existing geological results, including remotely sensed geological prospecting signs, remote sensing alteration abnormal signs, etc. According to the profile measurements taken in the field, clownology peridotite constitutes the most exposed lithology on the profile and is also the main ore-bearing rock body. It is strongly weathered, brownish yellow to and dark yellow-green in color, and has a hard fresh surface. The surface characteristics have been altered by the presence of pyroxene, and the rock is mainly composed of olivine, orthopyroxene, and chromium spinel. A chromite ore body is present in the clinopyroxene peridotite, which is massive and lenticular. The two are in a clearly contacting relationship at the direct contact [32]. However, close observation reveals that portions of the chromite and clinopyroxene have

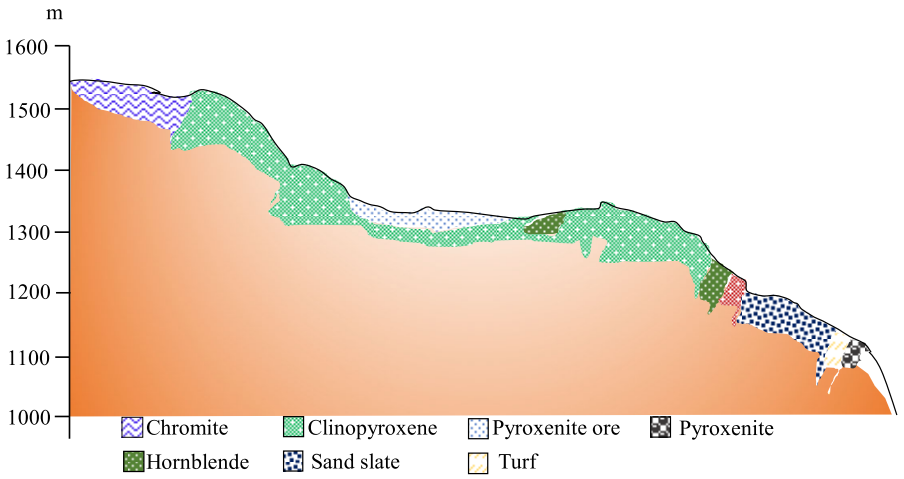

FIGURE 7. Measured plan map of the mining area.

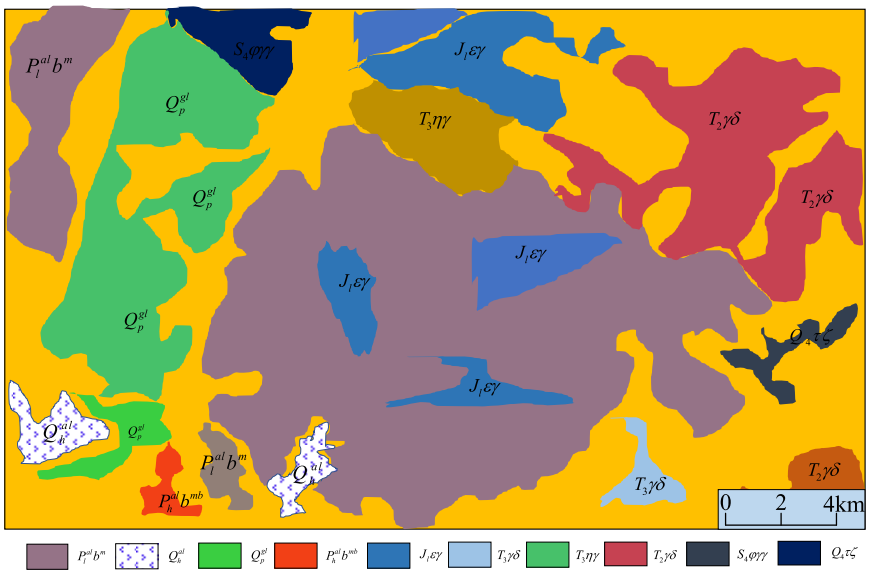

FIGURE 8. Geological survey map of the positioning area.

been serpentinized and contain a small amount of muddy alteration. There are structural fracture zones on both sides of the plagioclase peridotite, producing structural breccia, that reflect the close relationship between the ore-forming evolution of the deposit and the structure of the mining area. In addition, other components in the ophiolite suite, such as pyroxenite, gabbro and other pyroxenite, have been exposed on a small scale due to the superimposition of the tectonic action of the Himalayan orogeny. The measured plan map of the mining area is shown in Figure 7.

C. GEOLOGICAL CHARACTERISTICS OF THE DEPOSIT

Figure 8 shows the geological survey map of the positioning area. The solar copper polymetallic deposit in the Kartika area is the largest skarn-type ore deposit that has been discovered in the area, and it is mainly composed of three skarn-type ore belts. The skarn belt is produced in the contact zone between the Middle-Late Triassic granodiorite, other small and medium-sized rock bodies, and the Mismanage Group [33]. The deposit is controlled by the composite control of directional faults, small and medium-sized granodiorite rocks, and the contact zone of the Quanta Group marble strata. Ore-controlling fractures have the characteristics of multiphase activities and are found of a relatively large scale, which has obvious controlling effects on the production of small and medium intrusive rock masses. The ore bodies in the mining area are mainly consist of copper, copper-molybdenum, molybdenum, and iron, followed by zinc, copper-zinc, and iron-zinc. The ore bodies are mostly lenticular and lamellar, followed by other irregular shapes. The occurrences of ore bodies are mostly oriented, which is basically consistent with the occurrences of the surrounding rocks and skarn belts. The mineralization alteration zone is mainly composed of tremolite skarn, diopside skarn, diopside

garnet skarn and marble. In-zone alteration is dominated by arenization, followed by epidote, chlorite, silicification and calcite. Metallic minerals are mainly chalcopyrite, chalcocite, molybdenite, bornite, pyrite and magnetite. The length of the ore body is generally 100-800 m, the thickness is 2-24.9 m, and the average copper grade w (Cu) is 0.34%-4.28%.

D. REMOTE SENSING INTERPRETATION

1) REMOTE SENSING LITHOLOGY INTERPRETATION

The lithology of this area is relatively simple, and mainly consists of basic ultrabasic rocks and a small amount of clastic rocks and carbonate rocks. According to the geological data of the study area, combined with the metalloorganic characteristics of the laterite nickel deposits, the following lithologic units and interpretation marks of the ore-bearing laterite layers are established [34]–[36].

(1) Ultrabasic rocks, mainly serpentine and dunnite, are widely distributed in the area and are the parent rocks of the laterite nickel deposits. The images collected show a massive structure, made up of wide mountain bodies, round and subangular ridges, slope gully development, and no obvious directionality and exists mostly in the form of free relief. The color of the image is mainly dark gray green.

(2) Gabbro is associated with ultrabasic rocks and its occurrence is relatively scattered; it is the secondary parent rock for laterite nickel mineralization in the study area. In the image, the landform appears to be relatively gentle, uneven, fine, speckled, and light-yellow green in color.

(3) Quaternary eluvium, quaternary flood, and alluvium deposits are distributed along the piedmont gentle slopes and in the river lands, mostly in the form of in situ residual resulting from river undercutting erosion; the eluvium is mostly eroded. The obtained image shows a gentle terrain with uniform fine speckled veins (caused by the presence of a forest canopy). The underlying bedrock in the area is ultrabasic rock, and the residual layer shows an uneven grayish green to yellowish brown color. It includes riverbeds, floodplains, valley slopes and river terraces, which has destroyed the eluvium via cutting erosion. In the obtained image, the purple patches represent riverbanks and sandbanks, and the brown area represents the river terrace.

(4) Ultrabasic rock weathered laterite and residual laterite is the parent rock of the nickel-bearing laterite deposits, followed by gabbro. In hot and rainy environments, nickel-bearing parent rocks form weathering crusts on the surface or near surface after long-term weathering and leaching. When these crusts reach a certain scale and grade, it becomes a laterite deposit.

The interpretation mark of the remotely sensed lithology is shown in Figure 9. Based on a systematic geological survey of the study area, the strata boundaries with Quaternary eluvium, Quaternary alluvium, ultrabasic rock, and gabbro are delineated. It can be seen from the investigation results that ultrabasic rocks are widely distributed in this area, accounting for nearly 3/5 of the total study area. The Quaternary residual and Quaternary alluvial deposits are mainly distributed in the northwestern part of the study area, accounting for approximately 2/5 of the study area, and a small amount of gabbro is distributed in the southwestern part of the study area.

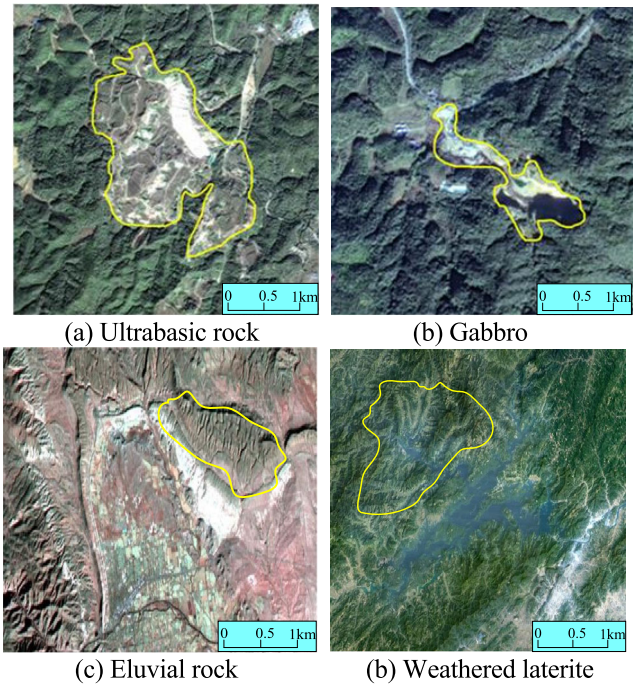

FIGURE 9. Interpretation mark of remote sensing lithology.

2) REMOTE SENSING INTERPRETATION OF MINERAL PROPERTIES

The screening of remote sensing alteration information mainly combines the information obtained from remote sensing geological interpretation and geological, geophysical, and geochemical data; it mainly eliminates the interference anomalies formed by some artificial features and retains the alteration information in the areas where intrusive rocks and linear structures are concentrated. The eigenvector of principal component analysis is shown in Table 1.

Table 2 describes the results of the principal component analysis. After comparative analysis and screening, most of these anomalies are determined to be distributed in the contact zone of the interpreted intrusive rock mass, skarn belt or fracture zone. Through field investigation, well developed skarn, chloritization, and petiotization are identified on the surface of the abnormal distribution area, and skarn-type lead-zinc mineralization signatures have been found in some areas. The carbonate rock section of the Ordovician-Silurian Tanisha group of the skarn type ore bearing strata is distributed sporadically across the area; a light gray white, uniform color, a straight ridge line, a medium water density system, a strip-shaped grain, a slightly tall mountain body, an obvious ridge line or steep cliff terrain, a collection of many gentle valleys, an obvious layered characteristic, a NWW trending distribution, and a pattern of patches and spots are indistinctly

TABLE 1. Eigenvector matrix of the principal component analysis of ETM.

Feature vector	EMT1	EMT4	EMT5	EMT7
PCA1	-0.945 371	-0.288 382	0.028 386	0.154 463
PCA2	0.211 786	-0.842 165	-0.298 156	-0.406 056
PCA3	-0.016 953	-0.197 618	-0.938 386	-0.287 532
PCA4	0.271 382	-423 713	0.178 872	-0.852 217

TABLE 2. Analysis table of principal components.

Principal components of information	Minimum value	Maximum value	Average value	Standard deviation
PCA4	-22.384 887	36.536 992	0.000 000	9.807 852

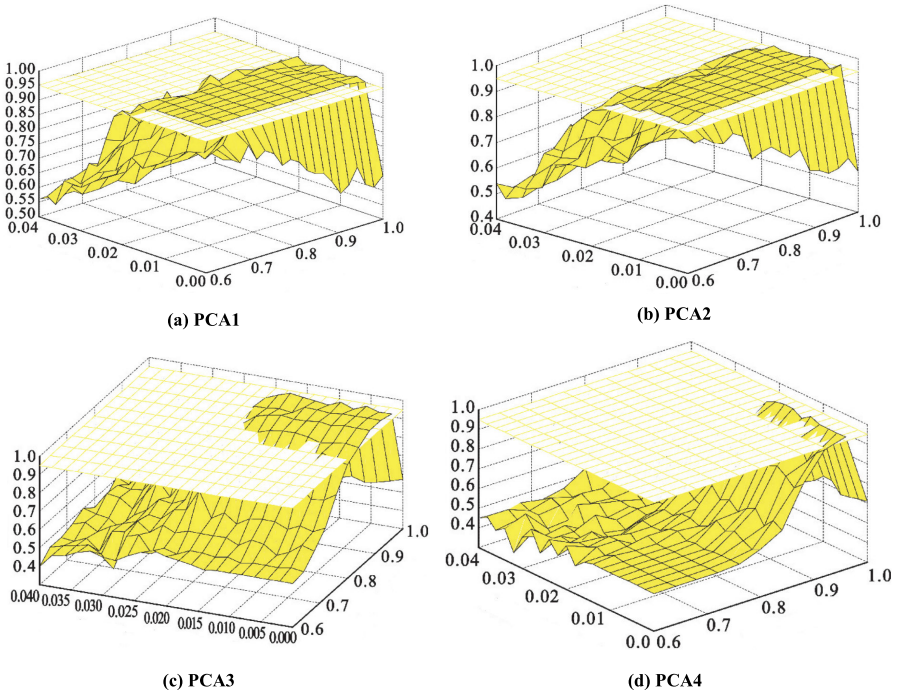

FIGURE 10. Comparison of the mineral content distribution based on principal component vector features.

visible. A comparison of the mineral content distribution based on the principal component vector feature is shown in Figure 10.

Abstractly speaking, remote sensing alteration information is systematized and theorized under the support of material information. The method of alteration information extraction is based on remoted sensing technologies, which use the spectral information of multiple bands and arranges the information from strongly to weakly predictive through orthogonal transformation. According to the spectral characteristics of altered minerals, selective principal component analysis is highly conducive to extracting weak geological information from remote sensing images. According to the relevant geological data, the altered minerals classified in the Lumbus chromite area mainly include hydroxyl-bearing minerals, such as serpentinized and iron staining alterations like magnetite and chromite. Therefore, based on an analysis of the spectral characteristics of the main altered minerals, bands such as the diagnostic spectra of altered minerals are selected for principal component analysis. Because the spectral diagnosis range of serpentinization is 2.3 μm and the minimum spectral resolution is less than 0.1 μm, it is difficult to accurately detect the spectral characteristics of serpentinized minerals in ETM. However, in high spatial resolution images, the hue anomaly of serpentinized areas can be used for interpretation. Field verification of the remote sensing interpretation of mineral properties is shown in Figure 11, and a comparison of the positioning accuracy and recall rate of the different ores observed is shown in Figure 12.

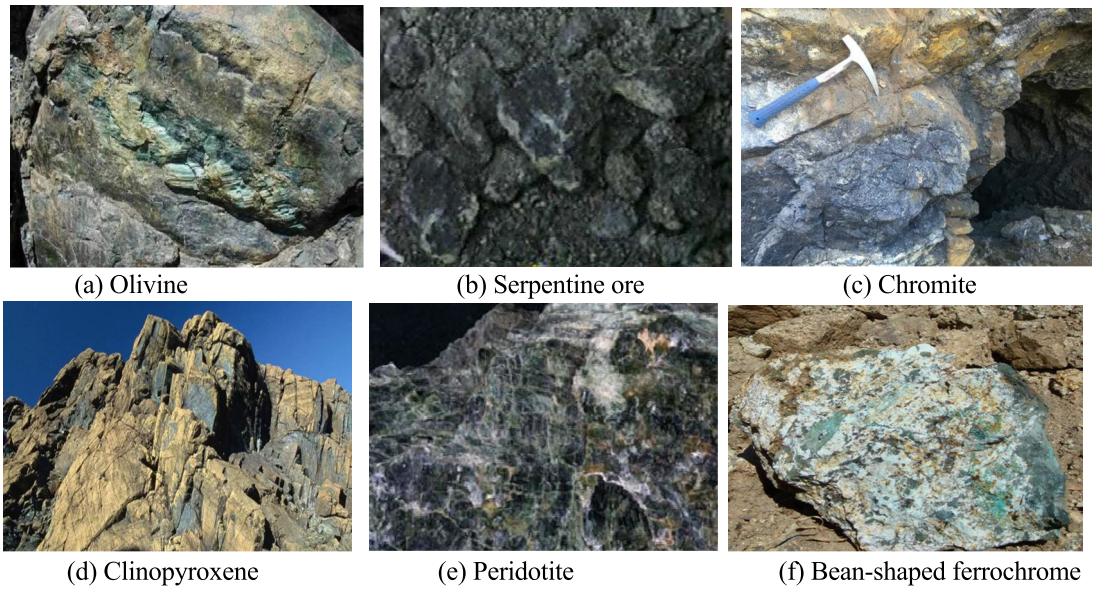

FIGURE 11. Field verification of the remote sensing interpretation of mineral properties.

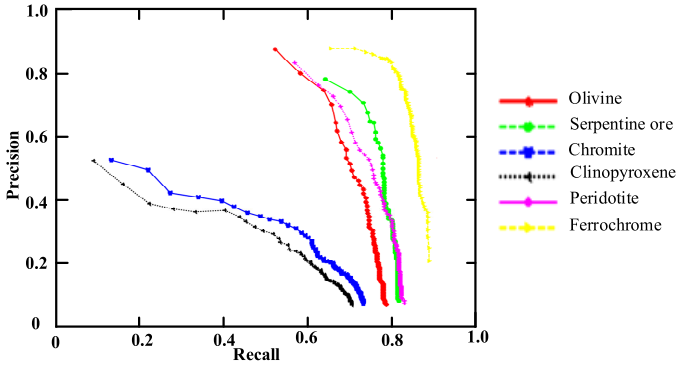

FIGURE 12. Comparison of the positioning accuracy and recall rate of the different ore types.

V. CONCLUSION

In this article, a method of locating ore deposits based on feature decomposition of high-resolution remote sensing images is proposed. High-resolution remote sensing images are used to extract the controlling factors of deposits. The color, shape, texture and other image shapes produced by high-resolution remotely sensed data are fully utilized to fully mine the data through mathematics, image processing methods and other technologies to comprehensively determine potential prospect target areas. Through the analysis of metalloorganic geological characteristics in the study area, the extracted color features, texture features and other elements are comprehensively analyzed. The logical superposition analysis method is used to obtain the intersection utilizing the theory of fuzzy mathematics, and the intersection position is the remote sensing prospecting target area. Making full use of the color, shape, texture and other image shapes shown by high-resolution remote sensing data, thus fully mining the data by using mathematics, image processing, and other technologies. This methodology was able to comprehensively determine the prospecting target area of the study site and provide a reliable basis for the peripheral exploration and deposit positioning of the mining area.

REFERENCES

[1] J. T. Zhu, C. F. Gong, M. X. Zhao, L. Wang, and Y. Luo, "Image mosaic algorithm based on Pac-orb feature matching," *Int. Arch. Photogramm., Remote Sens. Spatial Inf. Sci.*, vol. 42, pp. 83–89, Feb. 2020.

[2] Q. Huang, X. Feng, and P. Xiao, "An approach for linear feature detection from remote sensing images with high spatial resolution based on sparse decomposition," *Geomatics Inf. Ence Wuhan Univ.*, vol. 39, no. 8, pp. 913–917, 2014.

[3] Y. Li, J. W. Xu, J. F. Zhao, Y. D. Zhao, and X. Li, "An improved mean shift segmentation method of high-resolution remote sensing image based on LBP and canny features," *Appl. Mech. Mater.*, vols. 713–715, pp. 1589–1592, Jan. 2015.

[4] T. Delleji, A. Kallel, and A. Ben Hamida, "Iterative scheme for MS image pansharpening based on the combination of multi-resolution decompositions," *Int. J. Remote Sens.*, vol. 37, no. 24, pp. 6041–6075, Dec. 2016.

[5] A. Kallel, "MTF-adjusted pansharpening approach based on coupled multiresolution decompositions," *IEEE Trans. Geosci. Remote Sens.*, vol. 53, no. 6, pp. 3124–3145, Jun. 2015.

[6] S. Luo, L. Tong, Y. Chen, and L. Tan, "Landslides identification based on polarimetric decomposition techniques using Radarsat-2 polarimetric images," *Int. J. Remote Sens.*, vol. 37, no. 12, pp. 1–13, 2016.

[7] A. Sedaghat and N. Mohammadi, "High-resolution image registration based on improved SURF detector and localized GTM," *Int. J. Remote Sens.*, vol. 40, no. 7, pp. 2576–2601, Apr. 2019.
[8] M. Xu, M. Cong, T. Xie, Y. Tao, X. Zhu, and J. Zhao, "Unsupervised segmentation of high-resolution remote sensing images based on classical models of the visual receptive field," *Geocarto Int.*, vol. 30, no. 9, pp. 1–19, Feb. 2015.
[9] S. H. Xu, M. U. Xiaodong, Z. H. A. O. Peng, and M. A. Ji, "Scene classification of remote sensing image based on multi-scale feature and deep neural network," *Acta Geodaetica Cartograph. Sinica*, vol. 45, no. 7, pp. 834–840, Jul. 2016.
[10] X. Sun, H. Song, R. Wang, and N. Li, "High-resolution polarimetric SAR image decomposition of urban areas based on a POA correction method," *Remote Sens. Lett.*, vol. 9, no. 4, pp. 363–372, Apr. 2018.
[11] F. Xu, Y. Li, and Y.-Q. Jin, "Polarimetric–anisotropic decomposition and anisotropic entropies of high-resolution SAR images," *IEEE Trans. Geosci. Remote Sens.*, vol. 54, no. 9, pp. 5467–5482, Sep. 2016.
[12] Z. Shao, L. Wang, Z. Wang, and J. Deng, "Remote sensing image super-resolution using sparse representation and coupled sparse autoencoder," *IEEE J. Sel. Topics Appl. Earth Observ. Remote Sens.*, vol. 12, no. 8, pp. 2663–2674, Aug. 2019.
[13] N. Wen, S. Z. Yang, and S. C. Cui, "High resolution remote sensing image denoising based on curvelet-wavelet transform," *J. Zhejiang Univ.*, vol. 49, no. 1, pp. 79–86, 2015.
[14] X. Xie, Z. Xue, D. Wang, W. Liu, and P. Du, "Land cover classification in karst regions based on phenological features derived from a long-term remote sensing image series," *J. Remote Sens.*, vol. 19, no. 4, pp. 627–638, 2014.
[15] S. Iria, G. Navarro, M. Bolado-Penagos, F. Echevarría, and C. M. García, "High-chlorophyll-area assessment based on remote sensing observations: The case study of Cape Trafalgar," *Remote Sens.*, vol. 10, no. 2, pp. 165–168, 2018.
[16] X. Kang, S. Li, L. Fang, and J. A. Benediktsson, "Intrinsic image decomposition for feature extraction of hyperspectral images," *IEEE Trans. Geosci. Remote Sens.*, vol. 53, no. 4, pp. 2241–2253, Apr. 2015.
[17] Y. Chen, W. He, N. Yokoya, T.-Z. Huang, and X.-L. Zhao, "Nonlocal tensor-ring decomposition for hyperspectral image denoising," *IEEE Trans. Geosci. Remote Sens.*, vol. 58, no. 2, pp. 1348–1362, Feb. 2020.
[18] J. Tan, J. Zhang, and Y. Zhang, "Target detection for polarized hyperspectral images based on tensor decomposition," *IEEE Geosci. Remote Sens. Lett.*, vol. 14, no. 5, pp. 674–678, May 2017.
[19] S. Gu, S. Yan, H. Zhou, and J. Gong, "Super-resolution imaging based on the BeiDou B3 signal," *Int. J. Remote Sens.*, vol. 41, no. 6, pp. 2339–2358, Mar. 2020.
[20] H. He, X. Liu, and Y. Shen, "Relative radiometric correction of high-resolution remote sensing images based on feature category," *Cluster Comput.*, vol. 12, no. 3, pp. 1–9, 2018.
[21] Z. Bo and H. E. Binbin, "Multi-scale segmentation of high-resolution remote sensing image based on improved watershed transformation," *J. Geo-Inf. Sci.*, vol. 16, no. 1, pp. 142–150, 2014.
[22] Y. Run, M. Wang, Z. Dong, and Y. Cheng, "Urban road extraction of high resolution remote sensing image based on SLIC superpixel," *J. Geomatics*, vol. 44, no. 1, pp. 84–88, 2019.
[23] Q. Yan, H. Li, and L. H. Jing, "Automatic extraction algorithm of seismic landslide information based on after-calamity high-resolution remote sensing image," *Laser Optoelectron. Prog.*, vol. 54, no. 11, pp. 112–118, 2017.
[24] X. Wang, S. Liu, P. Du, H. Liang, J. Xia, and Y. Li, "Object-based change detection in urban areas from high spatial resolution images based on multiple features and ensemble learning," *Remote Sens.*, vol. 10, no. 2, pp. 276–280, 2018.
[25] M. Xu, C. O. N. G. Ming, W. A. N. Lijuan, X. I. E. Tianpeng, and Z. H. U. Xiaoling, "A methodology of image segmentation for high resolution remote sensing image based on visual system and Markov random field," *Acta Geodaetica Et Cartographica Sinica*, vol. 44, no. 2, pp. 198–205, 2015.
[26] G. Hu, X. Sun, D. Liang, and Y. Sun, "Cloud removal of remote sensing image based on multi-output support vector regression," *J. Syst. Eng. Electron.*, vol. 25, no. 6, pp. 1082–1088, Dec. 2014.
[27] N. Safina and M. Ehlers, "Building change detection using high resolution remotely sensed data and GIS," *IEEE J. Sel. Topics Appl. Earth Observ. Remote Sensing*, vol. 9, no. 8, pp. 3430–3438, May 2017.
[28] W. Zhou, S. Newsam, C. Li, and Z. Shao, "Learning low dimensional convolutional neural networks for high-resolution remote sensing image retrieval," *Remote Sens.*, vol. 9, no. 5, pp. 489–492, 2016.
[29] J. Chen, M. Deng, X. Mei, T. Chen, Q. Shao, and L. Hong, "Optimal segmentation of a high-resolution remote-sensing image guided by area and boundary," *Int. J. Remote Sens.*, vol. 35, no. 19, pp. 6914–6939, Oct. 2014.
[30] C. Liu, L. Hong, J. Chen, S. S. Chun, and M. Deng, "Fusion of pixel-based and multi-scale region-based features for the classification of high-resolution remote sensing image," *J. Remote Sens.*, vol. 19, no. 2, pp. 228–239, 2015.
[31] D. Chen, S. Shang, and C. Wu, "Shadow-based building detection and segmentation in high-resolution remote sensing image," *J. Multimedia*, vol. 9, no. 1, pp. 181–188, Jan. 2014.
[32] X. Zhang, P. Xiao, and X. Feng, "Fast hierarchical segmentation of high-resolution remote sensing image with adaptive edge penalty," *Photogramm. Eng. Remote Sens.*, vol. 80, no. 1, pp. 71–80, Jan. 2014.
[33] Z. Xiao, Y. Long, D. Li, C. Wei, G. Tang, and J. Liu, "High-resolution remote sensing image retrieval based on CNNs from a dimensional perspective," *Remote Sens.*, vol. 9, no. 7, pp. 725–728, 2017.
[34] M. Chen, S. Lu, and Q. Liu, "Uniform regularity for a Keller–Segel–Navier–Stokes system," *Appl. Math. Lett.*, vol. 107, Sep. 2020, Art. no. 106476.
[35] X. Pan and J. Zhao, "A central-point-enhanced convolutional neural network for high-resolution remote-sensing image classification," *Int. J. Remote Sens.*, vol. 38, no. 23, pp. 6554–6581, Dec. 2017.
[36] N. Zhang, X. Zhang, and L. Ye, "Tree crown extraction based on segmentation of high-resolution remote sensing image improved peak-climbing algorithm," *Trans. Chin. Soc. Agricult. Machinery*, vol. 45, no. 12, pp. 294–300, 2014.

SHULAN TANG was born in Inner Mongolia, China, in 1979. She received the bachelor's degree from the Xi'an University of Architecture and Technology, in 2002, and the master's degree from Chang'an University, in 2007, where she is currently pursuing the Ph.D. degree. She has published a total of nine articles. Her research interests include remote sensing and information technology.

JIANNONG CAO was born in Shanxi, China, in 1963. He received the bachelor's degree from Wuhan University, in 1987, the master's degree from Northwest University, in 2000, and the Ph.D. degree from Wuhan University, in 2005. His research interests include remote sensing and information technology.